applied sciences

MDPI

Article

NO Removal by Plasma-Enhanced NH_3-SCR Using Methane as an Assistant Reduction Agent at Low Temperature

Weixuan Zhao [1,2], Yanghaichao Liu [1,2], Heng Wei [3], Renxi Zhang [1,2,*], Gang Luo [1,2,*], Huiqi Hou [1], Shanping Chen [4] and Ruina Zhang [4]

1 Shanghai Key Laboratory of Atmospheric Particle Pollution and Prevention (LAP3), Institute of Environmental Science, Fudan University, Shanghai 200433, China
2 National Engineering Laboratory for VOCs Pollution Control Material & Technology, University of Chinese Academy of Sciences, Beijing 101408, China
3 Bao Wu Group Environmental Resources Technology Co., Ltd, Shanghai 200000, China
4 Shanghai Institute for Design & Research on Environmental Engineering, Shanghai 200232, China
* Correspondence: zrx@fudan.edu.cn (R.Z.); gangl@fudan.edu.cn (G.L.)

Received: 18 June 2019; Accepted: 2 July 2019; Published: 8 July 2019

Abstract: The effects of using CH_4 as an assistant reduction agent in plasma-assisted NH_3–SCR were investigated. The new hybrid reaction system performed better than DBD–NH_3–SCR when the O_2 concentration varied from 2% to 12%. Compared with DBD–NH_3–SCR, DBD–NH_3–CH_4–SCR (NH_3:CH_4 = 1:1) showed a more significant promotion effect on the performance and N_2 selectivity for NO_X abatement. When the O_2 concentration was 6% and the SIE was 512 J/L, the NO removal efficiency of the new hybrid system reached 84.5%. The outlet gas components were observed via FTIR to reveal the decomposition process and its mechanism. This work indicated that CH_4, as an assistant agent, enhances DBD–NH_3–SCR in excess oxygen to achieve a new process with significantly higher activity at a low temperature (≤348 K) for NO_X removal.

Keywords: dielectric barrier discharge (DBD); NO abatement; assistant reduction agent; DBD–SCR assisted by CH_4

1. Introduction

Nitrogen oxide (NO_X) emissions from fossil fuel combustion are one of the primary air pollutants, inducing various environmental problems, such as secondary aerosols and tropospheric ozone [1–4]. Hence, the abatement of NO_X is one of the most extensively studied fields in the history of environmental science. Selective catalytic reduction (SCR) is regarded as a practical method for the removal of NOx, which is highly efficient and environmentally friendly compared to other denitration methods. However, promising catalysts for NO_X reduction, such as Ag/Al_2O_3 [5–13] and Ce/Fe–ZSM-5 [14–18], have sufficient activity when the temperature exceeds 673 K. The V_2O_5–WO_3/TiO_2 [19–27] catalyst can achieve superior activity only when the temperature is between 573 K and 673 K. A high reaction temperature leads to expensive energy consumption and other problems [28,29]. Therefore, low temperature SCR has attracted much attention [30–32]. Many studies have demonstrated that low temperature (423–673 K) SCR could be achieved by changing the composition and support of the catalyst [33–36]. However, these modifications still have limitations, and finding a solution that can improve the low temperature activity of the SCR catalyst is necessary. Dielectric barrier discharge (DBD), one of the most promising normal temperature plasma (NTP) generation technologies, has also been proven to improve the activity of diverse SCR catalysts at low temperatures [37–41]. The technology of SCR assisted by DBD has received much attention in the past decade because it offers the advantages of

being highly efficient and eco-friendly with a distinguished performance on the decomposition of NOx [42–46].

SCR assisted by DBD provides synthesis effects to reach significantly higher activity than SCR when the temperature is lower than 673 K. However, there are some drawbacks to using NH_3 as a reducing agent in the DBD–SCR process. On the one hand, the negative effect of ammonia escape is unavoidable as a result of excess NH_3 in SCR. On the other hand, the excited oxygen atom activated by DBD in an excess of O_2 can react with NH_3 in the feed gas to produce secondary products and then weaken the reduction of NO_X in DBD–SCR [47–50]. Some studies have shown that the use of hydrocarbons as reducing agents in DBD–SCR could be of particular interest [51,52], not only for avoiding the production of ABS (ammonium bisulfate), but also for controlling the by-product of NO abatement. However, some limitations [53] are unavoidable in HC–SCR assisted by a DBD system, such as the production of coking.

Based on the superiority of hydrocarbons in DBD–SCR, using CH_4 as an assistant reducing agent in DBD–NH_3–SCR probably overcomes the negative effect of NH_3, which conduces the good performance of NO abatement for DBD–NH_3–SCR with exceeded O_2. Nevertheless, there are few reports concerning the effects of and mechanisms involved in plasma enhanced NH_3–SCR using methane as the assistant reducing agent in such a hybrid reaction system.

In this work, a new hybrid reaction system using CH_4 as an assistant reducing agent in DBD–NH_3–SCR has been studied in detail. The reaction products of NO abatement in DBD–SCR with different reducing agents were detected by Fourier transform infrared spectroscopy (FTIR). The selectivity of NO abatement for two hybrid systems has been researched and the involved chemical mechanism was also revealed.

2. Experimental Section

2.1. Materials

A V_2O_5–WO_3/TiO_2 catalyst, with a vanadium pentoxide content of 2% and a tungsten trioxide content of 9%, which had been prepared by a sol-gel method, was purchased from XinRui Co. (Hunan, CN) and was used without further purification.

2.2. Experimental Setup and Procedure

This experiment includes two type reactors of DBD–NH_3–SCR (DBD enhanced SCR with NH_3 as the reduction agent) and DBD–NH_3–CH_4–SCR (DBD enhanced SCR with NH_3 as the reduction agent and CH_4 as the assistant reduction agent). The feeding gas composition was 400 ppm of NO, 0–12% O_2, 0–90 ppm NH_3, 0–90 ppm CH_4, and N_2 as the balance gas to simulate the actual working conditions. The total flow rate and space velocity of the gas mixture were 15 L·min^{-1} and 66,000 h^{-1}, respectively. The mixed gases passed through a buffer chamber and then were led into the DBD reactor. The flow rate of each feeding gas was controlled independently by a mass flow controller (Dandong, Horiba Stec-4400, JPN). The reactor consisted of an inner high-voltage electrode (graphite), two quartz tubes (outer tube with 30 mm inner diameter and 200 mm length; inner tube with 6 mm outer diameter and 300 mm length), and an outer electrode (aluminum foil, thickness 0.2 mm). The quartz tubes were in the shape of coaxial cylinders with 12 mm gap. The length of the discharge area was 10 mm and the volume of the discharge area was 27 cm^3. The temperature of the discharge area was measured by infrared thermometer (Omega, OS423, GA, USA). The concentration of NO_3 was measured by ion chromatography (Thermo Fisher, DX-120, MA, USA).

The V_2O_5-WO_3/TiO_2 catalyst was performed in a fixed-bed (outer diameter, 30 mm), operating at atmospheric pressure. The fixed-bed was loaded onto a quartz wool at the center of the DBD reactor.

2.3. Analytical Measurements

The DBD power supply could provide a sinusoidal alternating voltage varying from 1 kV~4 kV at frequencies of 10 kHz~20 kHz. The voltage and power applied was measured via a 200 MHz digital phosphor oscilloscope (Tektronix, TDS2024B, Shanghai, China) connected to a 1000:1 HV probe (Tektronix, P6015A, OR, USA).

The concentration of all the gaseous components was continuously quantified using a Fourier transform infrared absorption spectrometer (FTIR 850, Gangdong Co., Tianjin, China, 0.5 cm^{-1}). The NO removal efficiency (η_{NO}) and N_2 selectivity (NO to N_2) were defined as follows:

$$\eta_{NO} = \frac{(NO_{inlet} - NO_{outlet})}{NO_{inlet}} \times 100\%;$$

$$N_2 \text{ selectivity } \% = \frac{NO_{inlet}+NH_{3inlet}-NO_{outlet}-2\times N_2O_{outlet}-NO_{2outlet}-NO_{3outlet}-NH_{3outlet}}{NO_{inlet}+NH_{3inlet}} \times 100\%,$$

where NO_{outlet}, N_2O_{outlet}, $NO_{2outlet}$, and $NO_{3outlet}$ are the concentrations (ppm) of NO, N_2O, NO_2, and NO_3 at the outlet of the reactor, respectively.

3. Results and Discussion

3.1. Performances of the DBD–NH_3–CH_4–SCR and DBD–NH_3–SCR Hybrid System

The effect of SIE (specific input energy) on the NO removal efficiency for the DBD–NH_3–CH_4–SCR and DBD–NH_3–SCR hybrid system is shown in Figure 1. A maximum NO conversion of approximately 70.5% was achieved at 512 J/L for the DBD–NH_3–SCR hybrid system, with 0% O_2 in the feed. The NO conversions ranged from 0% to 38.1% for the DBD–NH_3–CH_4–SCR hybrid systems.

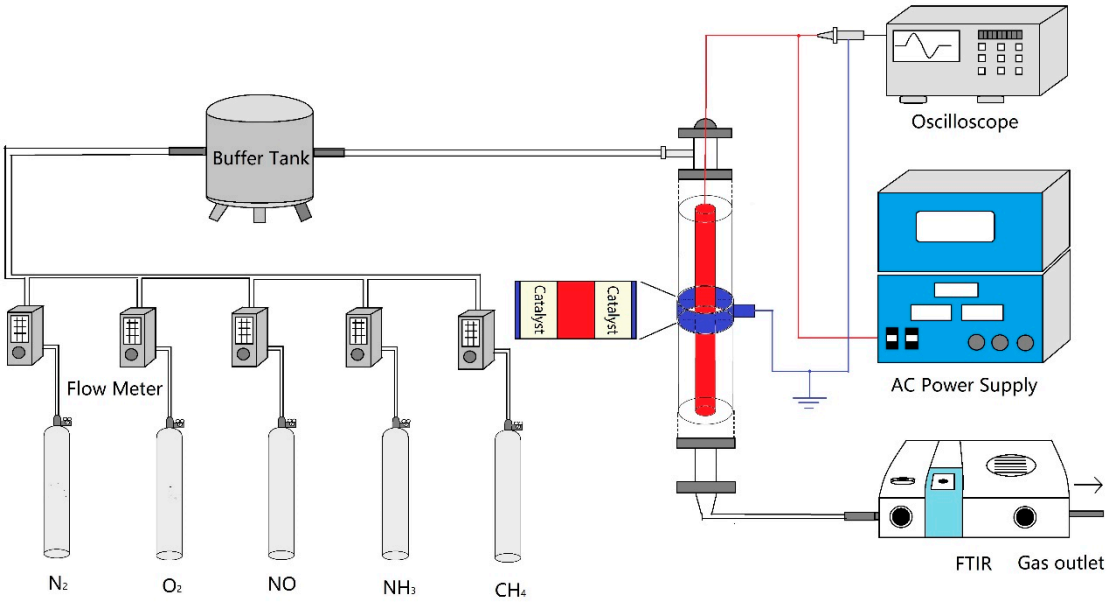

Figure 1. Schematic diagram of the experimental setup of the DBD–NH_3–CH_4–SCR system.

In the process of DBD–SCR, the temperature of the plasma reaction zone was determined by the SIE. In two cases, with the rise of SIE, the reaction temperature increased from 293 to 348 K. At 348 K, the experiment results indicated that no obvious NO conversion was found over the V_2O_5–WO_3 catalyst, only by thermal activation without DBD. Therefore, the heat effect of DBD on NO conversion can be neglected in this work.

The enhancement in SCR activation by plasma processes is generally attributed to the direct interaction of the radicals, electrons, and UV photons created by the plasma, with the catalyst and

molecules adsorbed on its surface. With the condition of O_2 absence, the reactions of NO + NO Ā→ N_2 + O_2 and NO + NH_2 → N_2 + H_2O cannot be ignored. Because NH_3 is more likely to be converted to NH_2 by DBD, as shown in Figure 2, the increasing SIE promoted NO conversion, and the performance of the DBD–NH_3–SCR hybrid system was better with O_2 free in the feed.

The overall conversion of NO in the presence of O_2 was presented in Figure 3. For the DBD–NH_3–SCR process, the NO conversion was reduced from 70.5% to 43.3%, with an increase in O_2 concentrations from 0% to 12%. Following the presence of methane in the reaction system, the results became different. For DBD–NH_3–CH_4–SCR, the NO conversion increased rapidly from 38.1% to 77% as the O_2 concentration reached 2%, and the NO conversion reached 85.2% when the O_2 concentration was 6%. In conclusion, the NO removal in the DBD–NH_3–SCR reactor was better than that in the DBD–NH_3–CH_4–SCR system with O_2 free; however, the opposite result was observed when the O_2 concentration was higher than 2%. This result indicates that O_2 has a negative effect on NO abatement in DBD–NH_3–SCR.

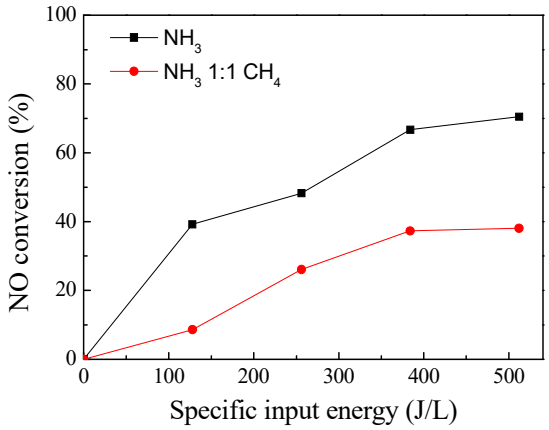

Figure 2. Effect of specific input energy (SIE) on the NO conversion of the DBD–NH_3–SCR and DBD–NH_3–CH_4–SCR processes. Reaction conditions: 400 ppm NO, O_2 free, balance N_2. (1) DBD–NH_3–SCR: 90 ppm NH_3. (2) DBD–NH_3–CH_4–SCR: 45 ppm CH_4 and 45 ppm NH_3.

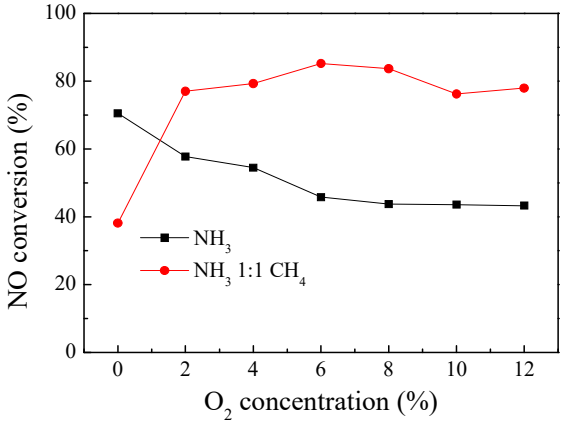

Figure 3. Effect of O_2 concentration on the NO conversion of the DBD–NH_3–SCR and DBD–NH_3–CH_4–SCR process. The SIE of DBD was kept at 512 J/L, O_2 concentration ranged from 0% to 12% and other reaction conditions were the same as those in Figure 2.

N_2O and NO_2 are known to be critical in the formation of N_2 in SCR reactions, and thus, the production of N_2O and NO_2 in the DBD–NH_3–SCR and DBD–NH_3–CH_4–SCR processes is also examined. The effect of SIE on N_2O and NO_2 concentration in the reaction system is shown in Figure 4a,b. For the DBD–NH_3–SCR process, the N_2O and NO_2 concentration is obviously higher than that in the DBD–NH_3–CH_4–SCR processes under the condition of 12% O_2. Therefore, these results

indicate that DBD–NH_3–CH_4–SCR had a lower production of N_2O and NO_2 and achieved better selectivity than DBD–NH_3–SCR in the condition of exceeded O_2.

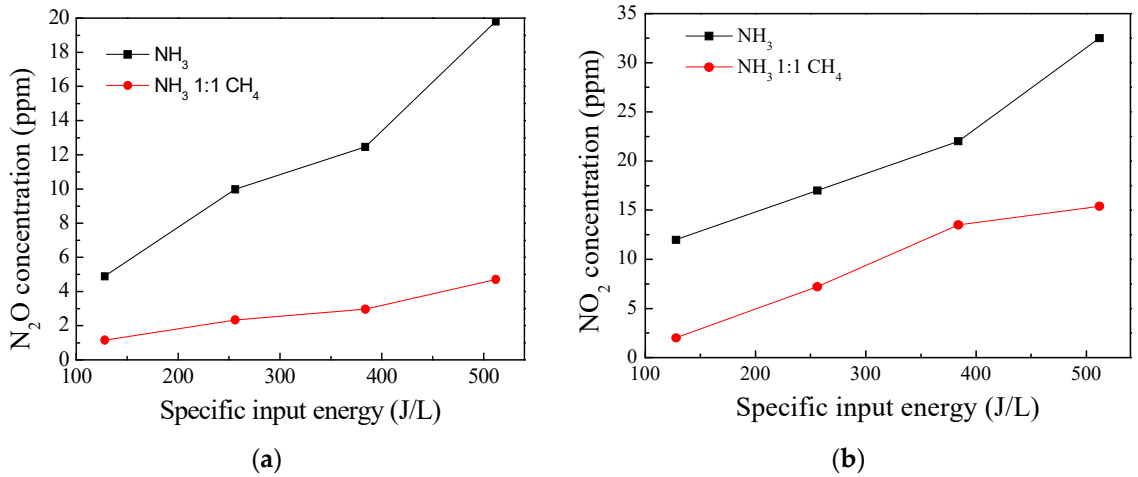

Figure 4. (**a**) N_2O concentration for DBD–SCR at SIE ranging from 128 J/L to 512 J/L. (**b**) NO_2 concentration for DBD–SCR at SIE ranging from 128 J/L to 512 J/L. Experimental conditions: 12% O_2, and other conditions are the same as those in Figure 2.

3.2. Effect of CH_4 and NH_3 on the Product Selectivity of the DBD–SCR Hybrid System

To explore the mechanisms involved, the products observed by FTIR in DBD–SCR are shown in Figure 5. Figure 5a shows the effect of SIE on NO abatement with 12% O_2 in the DBD–NH_3–SCR process. The NO concentration decreased gradually, however, the concentrations of N_2O and NO_2 increased obviously with increasing SIE. In addition, as shown in Figure 5b, the peak intensities of NO, NO_2, and N_2O, with peaks at 1900 cm^{-1}, 1600 cm^{-1}, and 2200 cm^{-1}, respectively, increased with increasing O_2 concentration.

Products detected in the DBD–NH_3–SCR process with the assistant agent CH_4 at different SIE and O_2 concentrations are shown in Figure 5c,d. These results show that there was less N_2O and NO_2 in the process compared with the results shown in Figure 5a,b under excess O_2. This result indicates that DBD–NH_3–SCR with CH_4 as an assistant reduction agent achieved a preferable performance and product selectivity for NO_X abatement.

To further verify and explore the above experimental results, the final products for the two DBD-catalyst systems with only NH_3/O_2 or N_2/O_2 in the feed are shown in Figure 6a,b, respectively. According to Figure 6a, N_2O (16.76 ppm) and NO_2 (10.97 ppm) were observed in the final products when the supplied gases only included NH_3, O_2, and N_2 balance gas. According to a previous research report [47], O_2 not only competitively shares the input power but also contributes to the oxidation of NO. NO, N_2, and NH_3 were dissociated by electron impact dissociation reactions in the discharge area, namely, $e + NO \rightarrow e + NO^*$, $e+N_2 \rightarrow e+2N$ and $e+NH_3 \rightarrow e+\cdot NH_2+\cdot H$. Excited N, NO^*, NH_3, and $\cdot NH_2$ would recombine with O and O_2 to produce new NO_X. However, according to Figure 6b, there was only O_3 (98.16 ppm) in the reaction system of N_2/O_2. This indicates that the electrons generated from the DBD–SCR reactors could not decompose N_2 in this reaction system, similar conclusions are studied in another paper [54].

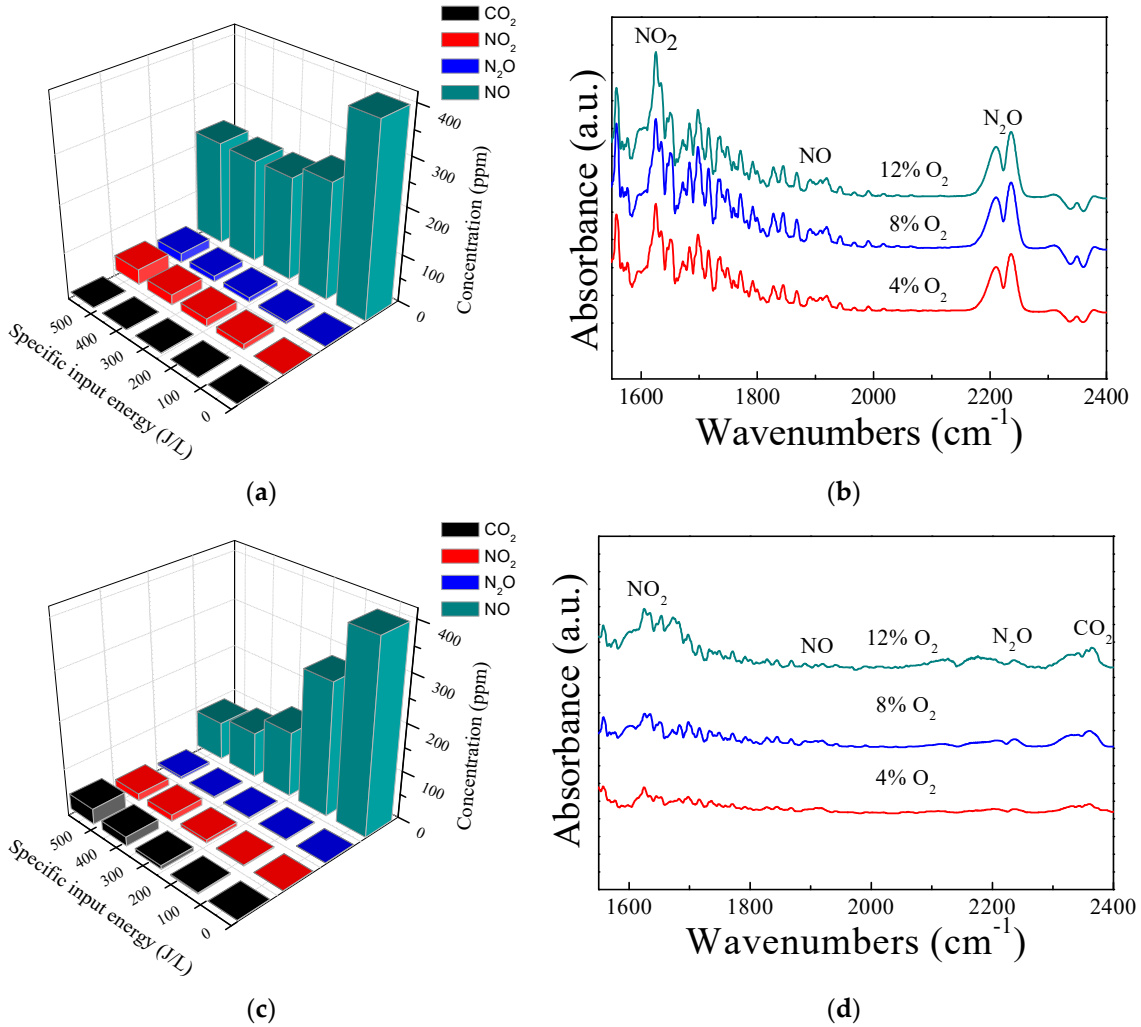

Figure 5. The product concentration and Fourier transform infrared spectroscopy (FTIR) spectra observed in different systems over V_2O_5–WO_3/TiO_2 with different O_2 and SIE. (**a**,**b**): DBD–NH_3–SCR, (**c**,**d**): DBD–NH_3–CH_4–SCR. Feed gas composition: 400 ppm NO, balance N_2 and 90 ppm NH_3 in DBD–NH_3–SCR, 45 ppm CH_4 and 45 ppm NH_3 in DBD–NH_3–CH_4–SCR.

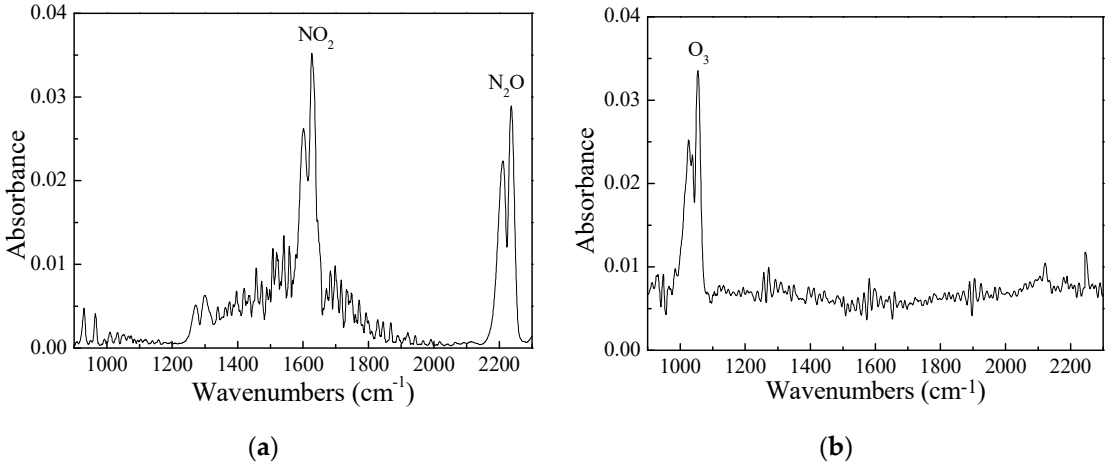

Figure 6. FTIR spectra of final products for the DBD-catalyst system with NH_3/O_2 and N_2/O_2 (reaction conditions: (**a**) 90 ppm NH_3, 12% O_2 and balance N_2; (**b**) 12% O_2 and 88% N_2).

Because NH_3 could recombine with excited O to produce new NO_X, it is an inevitable fact that O_2 has a negative effect on NO removal in DBD–NH_3–SCR, which is consistent with the results shown in Figure 3. On the contrary, the recombination of NH_3 and O_2 could be controlled in DBD–NH_3–CH_4–SCR. During plasma discharge, hydrocarbon could be decomposed and further generate useful intermediates, such as methyl ($\cdot CH_3$) and methyldioxy (CH_3O_2), which could react with NO molecules [55,56]. The enhancement in hydrocarbon activation by plasma processes is attributed to those active particles, and the entire activation reaction is given by:

$$CH_4 + 2NO + O_2 \rightarrow N_2 + 2H_2O + CO_2.$$

For this reason, CH_4 enhanced the removal efficiency of NO for DBD–SCR with excess O_2 and DBD–NH_3–CH_4–SCR achieves the best selectivity for NO abatement.

Table 1 shows the concentration of feed gas and product at outlet for DBD–NH_3–SCR and DBD–NH_3–CH_4-systems. According to this table, there were fewer N_2O, NO_2, and NO_3 in the outlet production of DBD–NH_3–CH_4–SCR. Furthermore, because the synthesis effects of DBD–SCR and assistant reductant agent, the N_2 selectivity of DBD–NH_3–CH_4–SCR reached 69.9%, while the N_2 selectivity of DBD–NH_3–SCR was only 31.2%.

Table 1. The N_2 selectivity and concentration of feed gas as well as products at outlet.

	Feed Gas Concentration of Inlet (ppm)		Product Concentration of Outlet (ppm)						N_2 Selectivity (%)
	NO	**CH_4**	**NH_3**	**NO**	**NO_2**	**N_2O**	**NO_3**	**NH_3**	
DBD–NH_3–SCR	400	0	90	220	32.5	19.8	37.2	7.7	31.2
DBD–NH_3–CH_4–SCR	400	45	45	80	15.4	4.71	25.5	3.8	69.9

Experiment condition: 12% O_2, SIE 512 J/L, the NO_3 was collected from outlet.

3.3. Effect of Different Ratios of CH_4 as An Assistant Agent on Final Products

The FTIR spectra for the reducing agent with different ratios of NH_3 and CH_4 under 2% O_2 are shown in Figure 7. They show that with the increase in the CH_4 proportion, N_2O decreased rapidly from 13.97 ppm to 0.80 ppm and there were few N_2O (0.80 ppm) products when the ratio of NH_3 and CH_4 was 1:1. This result indicates that the production of new NO_X could be controlled in DBD–NH_3–CH_4–SCR (NH_3:CH_4 = 1:1) with the favorable product selectivity.

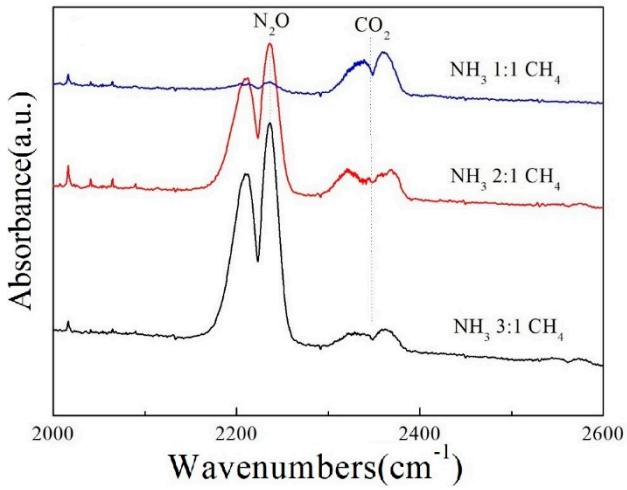

Figure 7. FTIR spectra and products detected in the DBD-NH_3-CH_4-SCR with different ratios of NH_3 and CH_4. Experimental conditions: 2% O_2, SIE 512 J/L, NH_3 1:1 CH_4: 45 ppm NH_3 and 45 ppm CH_4, NH_3 2:1 CH_4: 60 ppm NH_3 and 30 ppm CH_4, NH_3 3:1 CH_4: 67.5 ppm NH_3 and 22.5 ppm CH_4.

4. Reaction Mechanism

For NH_3–SCR, the reaction of NH_3 with NO occupied the main position in the reaction system. NH_3 could convert NO to N_2 by the reaction, $4NH_3 + 4NO + O_2 \rightarrow 4N_2 + 6H_2O$ [57]. However, the NO removal efficiency was unsatisfactory in DBD–NH_3–SCR with excess O_2, because high-energy electrons generated from DBD could excite NH_3, NO, and O_2 in the feed gas and produced high-energy particles, namely, $e + NO \rightarrow e + NO^*$, $e + O_2 \rightarrow e + 2O$, $e + NH_3 \rightarrow e + \cdot NH_2 + \cdot H$. Furthermore, excited NO^*, NH_3, and $\cdot NH_2$ recombined with O_2 as well as these high-energy particles on the catalyst surface to generate new NO_X through the reactions [54,57–59]:

$$NO^* + O \rightarrow NO_2;$$

$$NO_2 + O \rightarrow NO_3;$$

$$2NH_3 + 2O_2 \rightarrow N_2O + 3H_2O\ ;$$

$$4NH_3 + 4NO + 3O_2 \rightarrow 4N_2O + 6H_2O;$$

$$4NH_3 + 5O_2 \rightarrow 4NO + 6H_2O;$$

$$2 \cdot NH_2 + O_2 \rightarrow 2NO + 2H_2;$$

$$\cdot NH_2 + 2O \rightarrow NO + H_2O.$$

In DBD–NH_3–CH_4–SCR, except for the reaction of $4NH_3 + 4NO + O_2 \rightarrow 4N_2 + 6H_2O$, CH_4, as the assistant reduction agent, could react with NO and O_2 to convert NO to N_2, namely, $CH_4 + 2NO + O_2 \rightarrow N_2 + 2H_2O + CO_2$. Meanwhile, CH_4 was converted to $\cdot CH_3$, namely, $e + CH_4 \rightarrow e + CH_3 + \cdot H$ [60], which further produced $CH_3O_2\cdot$ as well as NO_2 and CO_2 [61]. Furthermore, NO_2, generated from NO oxidation by O and CH_3O_2 could react with NO as well as NH_3 to form N_2 and H_2O through the reaction: $NO + NO_2 + 2NH_3 \rightarrow 2N_2 + 3H_2O$. This is the fast-$NH_3$–SCR reaction, which has been verified to achieve effective reduction of NO_X to N_2 [62–64]. In addition, NO_2 could be oxidized to NO_3 in the DBD-system with excess O_2 as the reaction of $NO_2 + O \rightarrow NO_3$. Another byproduct of N_2O could react with $\cdot CH_3$, O and NO, such as the following reactions [65–67]:

$$\cdot CH_3 + N_2O \rightarrow CH_3O\cdot + N_2;$$

$$O + N_2O \rightarrow O_2 + N_2;$$

$$O + N_2O \rightarrow 2NO;$$

$$NO + N_2O \rightarrow NO_2 + N_2.$$

Taking all above-mentioned facts into account, the presence of NH_3/CH_4 in the feed gases significantly enhances the reduction of NO_X to N_2 and the product selectivity of NO abatement in DBD–NH_3–CH_4–SCR.

A schematic diagram of the main chemical reaction mechanism for DBD–SCR using CH_4 as the assistant agent is shown in Figure 8.

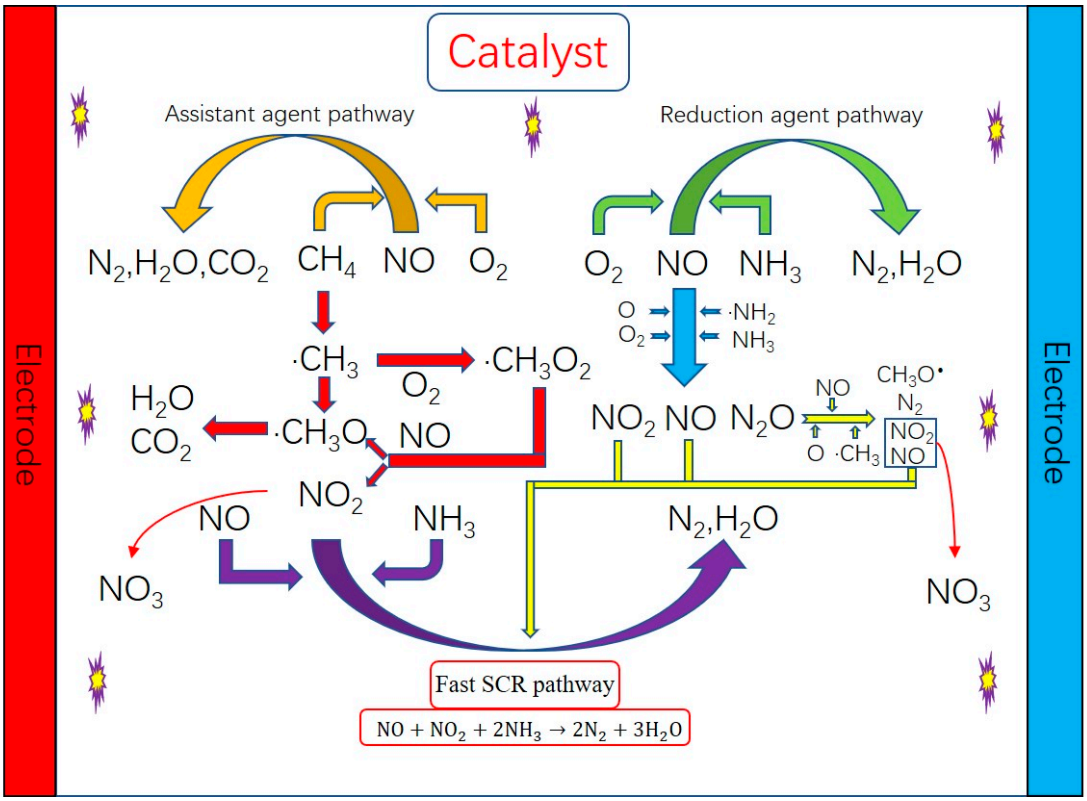

Figure 8. Schematic diagram of the main chemical reaction mechanism for the DBD–NH_3–SCR using CH_4 as an assistant agent.

5. Conclusions

NH_3–SCR assisted by DBD can enhance the NO_X conversion when CH_4 is used as an assistant reducing agent at low temperatures (below 348 K) with O_2 concentration exceeding 2%. The new hybrid reaction system overcomes the negative effect of the NH_3–SCR process, with a higher removal efficiency of NO and N_2 selectivity. The results of FTIR spectra observed in the new hybrid systems indicate that the DBD–NH_3–CH_4–SCR (NH_3:CH_4 = 1:1) had better synthesis effects and achieved a preferable performance as well as product selectivity for NO_X abatement. In addition, the fast-NH_3–SCR reaction was verified to achieve the important contribution for the reduction of NO_X to N_2 in the DBD–NH_3–CH_4–SCR system. Using CH_4 as an assistant reduction agent in plasma-assisted NH_3–SCR may provide a new idea for the NOx removal because the new process can effectively control secondary products and achieve a feasible low-temperature NO abatement technology with excess O_2.

Author Contributions: Conceptualization, W.Z. and Y.L.; Methodology, R.Z. (Renxi Zhang), G.L.; Validation, H.H. and H.W.; Formal Analysis, W.Z. and R.Z. (Ruina Zhang); Investigation, W.Z.; Resources, S.C.; Data Curation, W.Z.; Writing-Original Draft Preparation, W.Z.; Writing-Review & Editing, W.Z.; Visualization, Y.L.; Supervision, R.Z. (Renxi Zhang); Project Administration, G.L.; Funding Acquisition, S.C.

Funding: This research was funded by National Natural Science Foundation of China (Nos. 21577023), the Special Research Project on Causes and Control Technology of Air Pollution (Nos. 2017YFC0212905), and the science and technology innovation action Project supported by the Science and Technology Commission of Shanghai Municipality (Nos. 18DZ1202605).

Acknowledgments: The authors thank Jianyuan Hou and Yanghaichao Liu for their help in the research work.

Conflicts of Interest: The authors declare no conflict of interest.

References

1. Devahasdin, S.; Fan, C., Jr.; Li, K.; Chen, D.H. TiO_2, photocatalytic oxidation of nitric oxide: Transient behavior and reaction kinetics. *J. Photochem. Photobiol. A Chem.* **2003**, *156*, 161–170. [CrossRef]

2. Vestreng, V.; Ntziachristos, L.; Semb, A.; Reis, S.; Isaksen, I.S.A.; Tarrasón, L. Evolution of NOx emissions in Europe with focus on road transport control measures. *Atmos. Chem. Phys.* **2008**, *8*, 10697–10747. [CrossRef]
3. Forzatti, P. Present status and perspectives in de-NOx SCR catalysis. *Appl. Catal. A Gen.* **2001**, *222*, 221–236. [CrossRef]
4. Zhao, L.; Li, C.; Wang, Y.; Gao, L.; Zhang, J.; Zeng, G. Simultaneous removal of elemental mercury and NO from simulated flue gas using a CeO_2 modified V_2O_5–WO_3/TiO_2 catalyst. *Catal. Sci. Technol.* **2016**, *6*, 6076–6086. [CrossRef]
5. Burch, R.; Breen, J.; Meunier, F.; Meunier, F. A review of the selective reduction of NOx with hydrocarbons under lean-burn conditions with non-zeolitic oxide and platinum group metal catalysts. *Appl. Catal. B Environ.* **2002**, *39*, 283–303. [CrossRef]
6. He, H.; Yu, Y. Selective catalytic reduction of NOx over Ag/Al_2O_3 catalyst: From reaction mechanism to diesel engine test. *Catal. Today* **2005**, *100*, 37–47. [CrossRef]
7. Granger, P.; Pârvulescu, V.I. Catalytic NOxAbatement Systems for Mobile Sources: From Three-Way to Lean Burn after-Treatment Technologies. *Chem. Rev.* **2011**, *111*, 3155–3207. [CrossRef]
8. Shimizu, K.-I.; Satsuma, A. Selective catalytic reduction of NO over supported silver catalysts—Practical and mechanistic aspects. *Phys. Chem. Chem. Phys.* **2006**, *8*, 2677–2695. [CrossRef]
9. Liu, Z.; Woo, S.I. Recent Advances in Catalytic DeNOX Science and Technology. *Catal. Rev.* **2006**, *48*, 43–89. [CrossRef]
10. Liu, Z.; Li, J.; Junaid, A.S. Knowledge and know-how in improving the sulfur tolerance of deNOx catalysts. *Catal. Today* **2010**, *153*, 95–102. [CrossRef]
11. Burch, R. Knowledge and Know-How in Emission Control for Mobile Applications. *Catal. Rev.* **2004**, *46*, 271–334. [CrossRef]
12. Li, J.; Ke, R.; Li, W.; Hao, J. A comparison study on non-thermal plasma-assisted catalytic reduction of NO by C_3H_6 at low temperatures between Ag/USY and Ag/Al_2O_3 catalysts. *Catal. Today* **2007**, *126*, 272–278. [CrossRef]
13. Gunnarsson, F.; Pihl, J.A.; Toops, T.J.; Skoglundh, M.; Härelind, H. Lean NOx reduction over Ag/alumina catalysts via ethanol-SCR using ethanol/gasoline blends. *Appl. Catal. B Environ.* **2017**, *202*, 42–50. [CrossRef]
14. Salazar, M.; Hoffmann, S.; Singer, V. Hybrid catalysts for the selective catalytic reduction (SCR) of NO by NH_3. On the role of fast SCR in the reaction network. *Appl. Catal. B Environ.* **2016**, *199*, 433–438. [CrossRef]
15. Salazar, M.; Hoffmann, S.; Tkachenko, O.P.; Becker, R.; Grünert, W. Hybrid catalysts for the selective catalytic reduction of NO by NH_3: The influence of component separation on the performance of hybrid systems. *Appl. Catal. B Environ.* **2015**, *182*, 213–219. [CrossRef]
16. Salazar, M.; Becker, R.; Grünert, W. Hybrid catalysts—An innovative route to improve catalyst performance in the selective catalytic reduction of NO by NH_3. *Appl. Catal. B Environ.* **2015**, *165*, 316–327. [CrossRef]
17. Liese, T.; Löffler, E.; Grunert, W. Selective Catalytic Reduction of NO by Methane over CeO_2–Zeolite Catalysts—Active Sites and Reaction Steps. *J. Catal.* **2001**, *197*, 123–130. [CrossRef]
18. Salazar, M.; Hoffmann, S.; Tillmann, L.; Singer, V.; Becker, R.; Grünert, W. Hybrid catalysts for the selective catalytic reduction (SCR) of NO by NH_3: Precipitates and physical mixtures. *Appl. Catal. B Environ.* **2017**, *218*, 793–802. [CrossRef]
19. Lietti, L.; Forzatti, P.; Bregani, F. Steady-State and Transient Reactivity Study of TiO_2-Supported V_2O_5–WO_3De-NOxCatalysts: Relevance of the Vanadium−Tungsten Interaction on the Catalytic Activity. *Ind. Eng. Chem. Res.* **1996**, *35*, 3884–3892. [CrossRef]
20. Madia, G.; Elsener, M.; Koebel, M.; Raimondi, F.; Wokaun, A. Thermal stability of vanadia-tungsta-titania catalysts in the SCR process. *Appl. Catal. B Environ.* **2002**, *39*, 181–190. [CrossRef]
21. Weisweiler, W. Removal of NOx from automotive exhaust under lean conditions. *Symp. Diesel Mot. Technol.* **2000**, *72*, 441–449.
22. Alemany, L.J.; Ferlazzo, N.; Forzatti, P.; Lietti, L.; Giamello, E.; Bregani, F. Physico-chemical characterisation and catalytic behavior of V_2O_5-WO_3-TiO_2 catalysts. *J. Account. Audit. Financ.* **1995**, *31*, 593–614.
23. Chen, J.; Yang, R. Role of WO_3 in mixed V_2O_5-WO_3/TiO_2catalysts for selective catalytic reduction of nitric oxide with ammonia. *Appl. Catal. A Gen.* **1992**, *80*, 135–148. [CrossRef]
24. Ramis, G.; Busca, G.; Cristiani, C.; Lietti, L.; Forzatti, P.; Bregani, F. Characterization of tungsta-titania catalysts. *Langmuir* **1992**, *8*, 1744–1749. [CrossRef]

25. Kompio, P.G.; Brückner, A.; Hipler, F.; Manoylova, O.; Auer, G.; Mestl, G.; Grünert, W. V_2O_5-WO_3/TiO_2, catalysts under thermal stress: Responses of structure and catalytic behavior in the selective catalytic reduction of NO by NH_3. *Appl. Catal. B Environ.* **2017**, *217*, 365–377. [CrossRef]
26. Chen, L.; Li, J.; Ge, M. Poisoning effect of alkali metals doping over nano V_2O_5–WO_3/TiO_2 catalysts on selective catalytic reduction of NOx by NH_3. *Chem. Eng. J.* **2011**, *170*, 531–537. [CrossRef]
27. Zhang, S.; Zhong, Q. F-Doped V_2O_5-WO_3/TiO_2 as a Catalyst for NO Reduction with NH_3 at Low-Temperature. *IJESD Org.* **2012**, *3*, 441–445. [CrossRef]
28. Zhou, X.; Huang, X.; Xie, A.; Luo, S.; Yao, C.; Li, X.; Zuo, S. V_2O_5-decorated Mn-Fe/attapulgite catalyst with high SO_2 tolerance for SCR of NOx with NH_3 at low temperature. *Chem. Eng. J.* **2017**, *326*, 1074–1085. [CrossRef]
29. Gao, R.; Zhang, D.; Liu, X.; Shi, L.; Maitarad, P.; Li, H.; Zhang, J.; Cao, W. Enhanced catalytic performance of V_2O_5-WO_3/Fe_2O_3/TiO_2 microspheres for selective catalytic reduction of NO by NH_3. *Catal Sci. Technol.* **2013**, *3*, 191–199. [CrossRef]
30. Zhang, S.; Li, H.; Zhong, Q. Promotional effect of F-doped V_2O_5–WO_3/TiO_2 catalyst for NH_3-SCR of NO at low-temperature. *Appl. Catal. A Gen.* **2012**, *435*, 156–162. [CrossRef]
31. Damma, D.; Ettireddy, P.R.; Reddy, B.M.; Smirniotis, P.G. A Review of Low Temperature NH_3-SCR for Removal of NOx. *Catalysts* **2019**, *9*, 349. [CrossRef]
32. Damma, D.; Boningari, T.; Ettireddy, P.R.; Reddy, B.M.; Smirniotis, P.G. Direct Decomposition of NOx over TiO_2 Supported Transition Metal Oxides at Low Temperatures. *Ind. Eng. Chem. Res.* **2018**, *57*, 16615–16621. [CrossRef]
33. Martín, N.; Paris, C.; Vennestrøm, P.N.; Thøgersen, J.R.; Moliner, M.; Corma, A. Cage-based small-pore catalysts for NH_3-SCR prepared by combining bulky organic structure directing agents with modified zeolites as reagents. *Appl. Catal. B Environ.* **2017**, *217*, 125–136. [CrossRef]
34. Zhao, Z.; Yu, R.; Zhao, R.; Shi, C.; Gies, H.; Xiao, F.S.; De Vos, D.; Yokoi, T.; Bao, X.; Kolb, U.; et al. Cu-Exchanged Al-rich SSZ-13 Zeolite from Organotemplate-Free Synthesis as NH_3-SCR Catalyst: Effects of Na^+, Ions on the Activity and Hydrothermal Stability. *Appl. Catal. B Environ.* **2017**, *217*, 421–428. [CrossRef]
35. Beale, A.M.; Gao, F.; Lezcano-Gonzalez, I.; Peden, C.H.; Szanyi, J. Recent advances in automotive catalysis for NOx emission control by small-pore microporous materials. *Chem. Soc. Rev.* **2015**, *44*, 7371–7405. [CrossRef] [PubMed]
36. Li, J.; Chang, H.; Ma, L.; Hao, J.; Yang, R.T. Low-temperature selective catalytic reduction of NOx with NH_3 over metal oxide and zeolite catalysts—A review. *Catal. Today* **2011**, *175*, 147–156. [CrossRef]
37. Bai, M.; Leng, B.; Mao, S. Flue Gas Desulfurization by Dielectric Barrier Discharge. *Plasma Chem. Plasma Process.* **2016**, *36*, 511–521. [CrossRef]
38. Liu, H.; Wang, T.; Zhang, X.; Guo, Y.; Sun, B. Influence of the TiO_2/multi-walled carbon nanotubes (MWCNTs) mass ratio on NO removal over the Mn/TiO_2, (x)-MWCNTs (1 − x) catalyst assisted by plasma. *React. Kinet. Mech. Catal.* **2017**, *121*, 735–749. [CrossRef]
39. Wang, T.; Liu, H.; Zhang, X.; Guo, Y.; Zhang, Y.; Wang, Y.; Sun, B. A plasma-assisted catalytic system for NO removal over CuCe/ZSM-5 catalysts at ambient temperature. *Fuel Process. Technol.* **2017**, *158*, 199–205. [CrossRef]
40. Chen, J.X.; Pan, K.L.; Yu, S.J. Combined fast selective reduction using Mn-based catalysts and nonthermal plasma for NOx removal. *Environ. Sci. Pollut. Res.* **2017**, *24*, 1–13. [CrossRef]
41. Wang, J.; Yi, H.; Tang, X.; Zhao, S.; Gao, F.; Yang, Z. Oxygen plasma-catalytic conversion of NO over MnOx: Formation and reactivity of adsorbed oxygen. *Catal. Commun.* **2017**, *100*, 227–231. [CrossRef]
42. Guo, Y.; Liao, X.; Fu, M.; Huang, H.; Ye, D. Toluene decomposition performance and NOx by-product formation during a DBD-catalyst process. *J. Environ. Sci.* **2015**, *28*, 187–194. [CrossRef] [PubMed]
43. Wang, J.; Cai, Y.; Wang, J.; Zhang, L.; Li, X. Research on the Effect of C3H6 on NO Conversion Rate in a NTP Reactor. In Proceedings of the IEEE International Conference on Optoelectronics and Image Processing, Haiko, China, 11–12 November 2010; pp. 297–300.
44. Anaghizi, S.J.; Talebizadeh, P.; Rahimzadeh, H.; Ghomi, H. The Configuration Effects of Electrode on the Performance of Dielectric Barrier Discharge Reactor for NOx, Removal. *IEEE Trans. Plasma Sci.* **2015**, *43*, 1944–1953. [CrossRef]
45. Cho, B.K.; Lee, J.H.; Crellin, C.C.; Olson, K.L.; Hilden, D.L.; Kim, M.K.; Kim, P.S.; Heo, I.; Oh, S.H.; Nam, I.S.; et al. Selective catalytic reduction of NOx, by diesel fuel: Plasma-assisted HC/SCR system. *Catal. Today* **2012**, *191*, 20–24. [CrossRef]

46. Lee, D.H.; Lee, J.O.; Kim, K.T. Characteristics of plasma-assisted hydrocarbon SCR system. *Int. J. Hydrogen Energy* **2011**, *36*, 11718–11726. [CrossRef]
47. Sun, Q.; Zhu, A.-M.; Yang, X.; Niu, J.; Xu, Y. Formation of NOx from N_2 and O_2 in catalyst-pellet filled dielectric barrier discharges at atmospheric pressure. *Chem. Commun.* **2003**, *12*, 1418. [CrossRef]
48. Kim, H.-H.; Ogata, A.; Futamura, S. Effect of different catalysts on the decomposition of VOCs using flow-type plasma-driven catalysis. *IEEE Trans. Plasma Sci.* **2006**, *34*, 984–995. [CrossRef]
49. Liu, Y.; Zhang, R.; Hou, H.; Zhang, R. NO reduction using low-temperature SCR assisted by a DBD method. *Plasma Sci. Technol.* **2018**, *20*, 014002. [CrossRef]
50. Miessner, H.; Francke, K.P.; Rudolph, R.; Hammer, T. NOX, removal in excess oxygen by plasma-enhanced selective catalytic reduction. *Catal. Today* **2002**, *75*, 325–330. [CrossRef]
51. Guan, B.; Lin, H.; Cheng, Q.; Huang, Z. Removal of NOx with selective catalytic reduction based on nonthermal plasma peroxidation. *Ind. Eng. Chem. Res.* **2011**, *50*, 5401–5413. [CrossRef]
52. Fan, H.Y.; Shi, C.; Li, X.S.; Yang, X.F.; Xu, Y.; Zhu, A.M. Low-temperature NOx selective reduction by hydrocarbons on H-Mordenite catalysts in dielectric barrier discharge plasma. *Plasma Chem. Plasma Process.* **2009**, *29*, 43–53. [CrossRef]
53. Pan, H.; Guo, Y.; Jian, Y.; He, C. Synergistic Effect of Non-thermal Plasma on NOx Reduction by CH_4 over an In/H-BEA Catalyst at Low Temperatures. *Energy Fuels* **2015**, *29*, 5282–5289. [CrossRef]
54. Zhao, W.; Wang, F.; Liu, Y.; Zhang, R.; Hou, H. Effects of Electrode Structure and Electron Energy on Abatement of NO in Dielectric Barrier Discharge Reactor. *Appl. Sci.* **2018**, *8*, 618. [CrossRef]
55. Nie, Y.; Wang, J.Y.; Zhong, K.; Wang, L.M.; Guan, Z.C. Synergy study of plasma-facilitated C_2H_4 selective catalytic reduction of NOx over Ag/γ-Al_2O_3 catalyst. *IEEE Trans. Plasma Sci.* **2007**, *35*, 663–669. [CrossRef]
56. Wang, X.Q.; Li, Y.; Chen, W.; Lv, G.H.; Huang, J.; Zhu, G.X.; Wang, X.Q.; Zhang, X.H.; Wang, D.C.; Feng, K.C.; et al. Characteristics of NOx removal combing dielectric barrier discharge plasma with selective catalytic reduction by C_2H_5OH. *J. Appl. Phys.* **2009**, *106*, 013309. [CrossRef]
57. Marberger, A.; Ferri, D.; Elsener, M.; Sagar, A.; Artner, C.; Schermanz, K.; Kröcher, O. Relationship between structures and activities of supported metal vanadates for the selective catalytic reduction of NO by NH_3. *Appl. Catal. B* **2017**, *218*, 731–742. [CrossRef]
58. Cobos, C.J.; Hippler, H.; Troe, J. The Reaction of NH_2 + O_2 at High Temperatures. *J. Phys. Chem.* **1995**, *99*, 342–349.
59. Cohen, N.; Westberg, K.R. Chemical Kinetic Data Sheets for High-Temperature Reactions. Part II. *J. Phys. Chem. Ref. Data* **1991**, *20*, 1211–1311. [CrossRef]
60. Nishida, Y.; Chen, T.-C.; Cheng, C.-Z. Effects of Multiple Pulses on Decomposition of Hydrocarbons for Hydrogen Production. *IEEE Trans. Plasma Sci.* **2018**, *46*, 962–966. [CrossRef]
61. Lin, H.; Guan, B.; Cheng, Q.; Huang, Z. An Investigation on the Principal Paths to Plasma Oxidation of Propylene and NO. *Energy Fuels* **2010**, *24*, 5418–5425. [CrossRef]
62. Jabłońska, M.; Delahay, G.; Kruczała, K.; Błachowski, A.; Tarach, K.A.; Brylewska, K.M.; Petitto, C.; Góra-Marek, K. Standard and Fast Selective Catalytic Reduction of NO with NH_3 on Zeolites Fe-BEA. *J. Phys. Chem. C* **2016**, *120*, 16831–16842. [CrossRef]
63. Koebel, M.; Madia, G.; Raimondi, F.; Wokaun, A. Enhanced Reoxidation of Vanadia by NO_2 in the Fast SCR Reaction. *J. Catal.* **2002**, *209*, 159–165. [CrossRef]
64. Cao, L.; Chen, L.; Wu, X.; Ran, R.; Xu, T.; Chen, Z.; Weng, D. TRA and DRIFTS studies of the fast SCR reaction over CeO_2/TiO_2 catalyst at low temperatures. *Appl. Catal. A Gen.* **2018**, *557*, 46–54. [CrossRef]
65. Tomeczek, J.; Gradoń, B. The role of N_2O and NNH in the formation of NO via HCN in hydrocarbon flames. *Combust. Flame* **2003**, *133*, 311–322. [CrossRef]
66. Nancy, E.; Meagher, W.R. Anderson. Kinetics of the O(3P) + N_2O Reaction. 2. Interpretation and Recommended Rate Coefficients. *J. Phys. Chem. A* **2000**, *104*, 6013–6031.
67. Mebel, A.M.; Lin, M.C.; Morokuma, K.; Melius, C. Theoretical study of reactions of N_2O with NO and OH radicals. *Int. J. Chem. Kinet.* **1996**, *28*, 693–703. [CrossRef]